Microstructure and Porosity of Laser Welds in Cast Ti-6Al-4V with Addition of Boron

Citation for the original published paper (version of record):
Tolvanen, S., Pederson, R., Klement, U. (2018)
Microstructure and Porosity of Laser Welds in Cast Ti-6Al-4V with Addition of Boron
Metallurgical and Materials Transactions A: Physical Metallurgy and Materials Science, 49(5): 1683-1691
http://dx.doi.org/10.1007/s11661-018-4543-1

Microstructure and Porosity of Laser Welds in Cast Ti-6Al-4V with Addition of Boron

SAKARI TOLVANEN, ROBERT PEDERSON, and UTA KLEMENT

Addition of small amounts of boron to cast Ti-6Al-4V alloy has shown to render a finer microstructure and improved mechanical properties. For such an improved alloy to be widely applicable for large aerospace structural components, successful welding of such castings is essential. In the present work, the microstructure and porosity of laser welds in a standard grade cast Ti-6Al-4V alloy as well as two modified alloy versions with different boron concentrations have been investigated. Prior-β grain reconstruction revealed the prior-β grain structure in the weld zones. In fusion zones of the welds, boron was found to refine the grain size significantly and rendered narrow elongated grains. TiB particles in the prior-β grain boundaries in the cast base material restricted grain growth in the heat-affected zone. The TiB particles that existed in the as cast alloys decreased in size in the fusion zones of welds. The hardness in the weld zones was higher than in the base material and boron did not have a significant effect on hardness of the weld zones. The fusion zones were smaller in the boron-modified alloys as compared with Ti-6Al-4V without boron. Computed tomography X-ray investigations of the laser welds showed that pores in the FZ of the boron modified alloys were confined to the lower part of the welds, suggesting that boron addition influences melt pool flow.

https://doi.org/10.1007/s11661-018-4543-1

I. INTRODUCTION

COMPARED with most other metallic materials, titanium alloys show superior specific strength and fatigue resistance.[1] This makes them advantageous in applications where light weight is an important parameter, such as in aerospace. Lighter components result in lower fuel consumption, which decreases both the environmental impact as well as costs. To be able to build optimal components, with regard to both cost effectiveness and lightweight design, welding is one of the key technologies for manufacture of large structural parts for aerospace applications.

The microstructure of welded α-β titanium alloys is typically characterized by coarse prior-β grains occasionally with a continuous α layer in the prior-β grain boundaries, and an acicular microstructure consisting of fine α' and/or α plates separated by thin layers of β phase.[2,3] The fine acicular microstructure contributes to the high strength of additively manufactured and welded titanium alloys but, on the other hand, these aspects reportedly contribute to the lowered ductility of Ti-6Al-4V welds.[4–6] Recent work[7–9] has indicated that addition of a small amount of boron to a titanium alloy can render a significantly finer microstructure in cast titanium alloys. Similar observations have been reported[10–12] in additive manufacturing where boron addition has been shown to refine the otherwise typically coarse columnar prior-β grain morphology. Reconstruction of the β grains, using the electron back scatter diffraction data of α phase, has proven to be a powerful method to characterize prior-β grain structure in titanium alloys.[13–15]

In the present work, the influence of boron addition in titanium alloy laser beam welds is explored. The titanium alloy investigated here is the α-β alloy Ti-6Al-4V, and two modified versions of it with 0.06 wt pct B and 0.11 wt pct B addition, respectively. The same welding process parameters were used when welding the different alloy compositions. The following selected key features were investigated and quantitatively characterized with regard to the effect of boron addition: (i) prior-β grain size and α phase morphology in the weld zones, (ii) the porosity in the fusion zone, (iii) the weld geometry, and (iv) the effect of welding on the TiB particle size and distribution.

SAKARI TOLVANEN is with the Department of Industrial and Materials Science, Chalmers University of Technology, 41296 Gothenburg, Sweden. Contact e-mail: sakari.tolvanen@chalmers.se ROBERT PEDERSON is with the Department of Industrial and Materials Science, Chalmers University of Technology and also with the Department of Engineering Science, University West, 46186 Trollhttan, Sweden. UTA KLEMENT is with the Department of Industrial and Materials Science, Chalmers University of Technology.

Manuscript submitted October 25, 2017.
Article published online March 12, 2018

II. MATERIALS AND METHODS

The welding experiments were performed on 8.5-mm-thick sections cut out from Ti-6Al-4V (hereafter called Ti-64) cast ingots with different boron contents. The cast materials for this study were supplied by Titanium Castings Ltd, UK. The results of the characterization of the castings have been published previously.[6] The chemical compositions of the three different alloys are provided in Table I. Boron was added in the form of TiB_2 particles in the size range of 1.7 to 5 mm. After casting, the ingots were hot isostatically pressed (HIP) at 900 °C with 100 MPa for 2 hours.

Bead on plate laser welds were conducted on 8.5-mm-thick sections of each alloy composition. Figure 1 shows bead on plate welds on the standard grade Ti-6Al-4V cast section. Laser weld 1 was investigated in the present work. Similar welds were made in the two Ti-64 alloy variants with boron addition. After welding, the weld cross sections were examined to investigate the weld geometry, microstructure, and micro hardness. Hereafter, the laser welds are designated L-0B, L-0.06B, and L-0.11B to indicate the amount of boron, *i.e.,* 0 wt pct B, 0.06 wt pct B or 0.11 wt pct B, respectively.

Sample preparation was done using conventional metallographic techniques for titanium alloys, including grinding and polishing. For optical microscopy, samples were etched with Kroll's etchant.

Scanning electron microscopy (SEM) and electron backscatter diffraction (EBSD) analyses were performed with a Zeiss Leo Gemini 1550 SEM. A 4 μm step size was used to acquire overview EBSD maps across the fusion zone (FZ), the heat-affected zone (HAZ), and in the base material (BM). Based on the existence of the Burgers orientation relationship between the body-centered cubic β phase and the hexagonal α phase, a numerical reconstruction of the parent β grains from the room temperature α phase EBSD data was performed using Merengue 2 software. A complete description of the reconstruction procedure can be found elsewhere.[12]

For quantitative image analysis, unetched samples were examined using backscatter electrons. ImageJ software was used to determine the length and thickness of α-laths and the size and volume fraction of TiB particles. The dimensions of fusion zones and heat-affected zones, as well as the spacings between TiB particles were measured, using optical microscopy.

Vickers hardness measurements were performed with a Shimadzu HMV-2000 hardness tester using a load of 500 g for 12 seconds and a Wolpert 2RC hardness tester using a load of 5 kg for 12 seconds. The hardness was measured in the FZ, the HAZ, and the BM, respectively. The shown values are an average of a minimum of 20 measurements.

The porosity in the welds was examined with a Nikon XTEK XTH 225kV X-ray microtomography system. A 27-mm-long section of each laser weld was scanned and the dimensions of the examined volumes were approximately 8.5 × 8.5 × 27 mm. The reconstruction was done using a voxel size of 5 μm. The X-ray tube settings (180 kV, 130 μA) produce a focal spot size of approximately 20 to 25 μm. The geometric enlargement was 23.5× and detector pixel size was 127 μm. With these conditions, the geometric unsharpness is 0.5 mm and the smallest detectable defect size is approximately 20 μm.

III. RESULTS

A. *Overview Microstructure*

Figure 2 shows the laser weld cross sections in Ti-64 with and without boron, with the different weld zones indicated in Figure 2(c). The fusion line is clearly visible in samples with boron (Figures 2(b) and (c)) but difficult to discern in Ti-64 weld not alloyed with boron. The welds were fully penetrated through the 8.5-mm-thick sections, wider at the top and bottom, and characterized by a narrow waist in the middle. The width of the FZs was measured at the top and at the bottom of the weld, as indicated in Figure 2(c). As shown in Table II, the maximum width of FZs varied between 4.4 and 5.9 mm. The width of the FZs seemed to decrease in the materials that contain boron. The HAZ was the widest at the top and gets narrower towards the bottom. The width of the HAZ was determined as the width of the region that had transformed to β-phase. The BM outside this area was also heat affected and slightly coarsened and can be seen

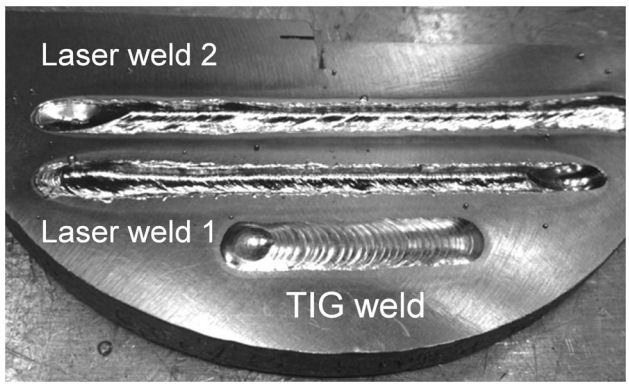

Fig. 1—Bead on plate welds Ti-64 cast material. Laser weld 1 was investigated in the present work.

Table I. Chemical Composition (in Weight Percent) of Cast Ti-64 Alloy and Its Variants Investigated in this Work

Alloy	Al	V	B	O	Fe	C	N	H	Y	Ti
Ti-64	6.16	4.04	< 0.001	0.20	0.20	0.010	0.002	< 0.001	< 0.001	bal.
Ti-64-0.06B	6.24	4.06	0.06	0.19	0.18	0.012	0.003	< 0.001	< 0.001	bal.
Ti-64-0.11B	6.18	4.02	0.11	0.24	0.19	0.007	0.004	< 0.001	< 0.001	bal.

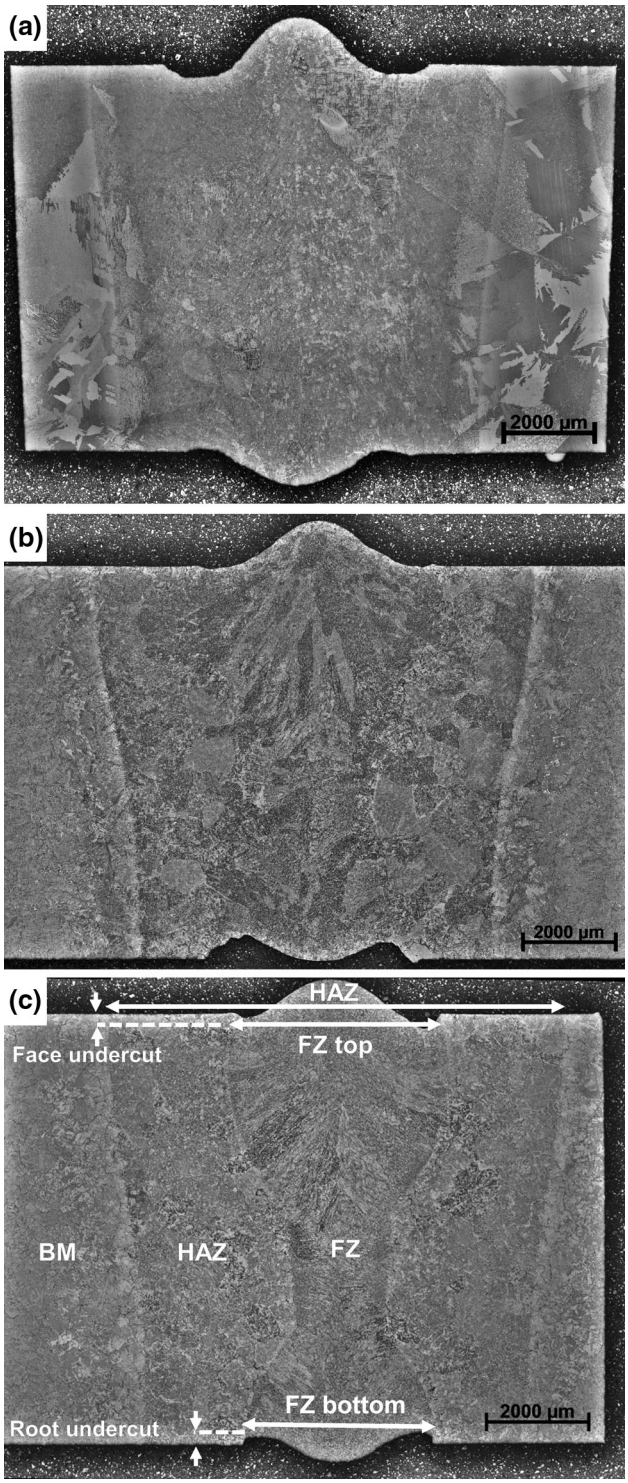

Fig. 2—Etched cross sections of (*a*) L-0B, (*b*) L-0.06B, and (*c*) L-0.11B.

outside the HAZ in Figure 2. Boron did not seem to have an effect on the width of HAZ. The face undercut seemed to be larger and the root undercut smaller in L-0B than in the boron alloyed welds.

Prior-β grains in L-0B weld appeared to be of the order of millimeters in size and span across the entire weld. In boron alloyed welds, the prior-β grain size, even though more difficult to distinguish, appeared to be significantly smaller. The prior-β grain size in BM was ranging from 1700 μm in standard grade Ti-64 to 200 μm in Ti-64 with 0.11 wt pct B.

Table III presents the micro and macro hardness results in different zones of the welds. Each value in the table is an average of a minimum of 20 measurements. The results show that FZ and HAZ have increased hardness compared to BM, with the highest hardness being in the HAZ in all the welds. The hardness of FZ, HAZ, and BM increased slightly with increasing boron content.

B. *Morphology and Distribution of TiB Particles*

Boron has very low solubility in titanium and, therefore, TiB particles are formed upon solidification.[7,8] In the cast BM, TiB particles were mainly observed at the prior-β grain boundaries. TiB particles in the BM and in the HAZ had an average length of approximately 30 to 50 μm and a thickness of 0.8 to 2.0 μm. In the FZ, the TiB particles were evenly distributed throughout the microstructure and their volume fraction increased with increasing boron solute concentration. TiB particles were found along the interdendritic regions forming stripes throughout the FZ as shown in Figure 3. The maximum length of TiB particles in the FZ was approximately 10 μm and the thickness of approximately 0.25 to 0.4 μm. As shown in Table IV, the spacing between the stripes was approximately 20 μm and did not vary significantly with amount of boron.

In the HAZ, further away from the FZ, the TiB particles were unaffected (Figure 3(d)). Approximately within 300 μm distance from the fusion zone boundary (Figure 3(c)), the morphology of TiB particles changed because of the heat from the welding process. Here, the TiB precipitates are broken up and their size was about 10 times smaller than that in the BM while still located along the prior-β grain boundaries. This indicates that changes, possibly melting or dissolution of TiB particles, occur along the prior-β grain boundaries while the β-grains remain in solid state.

C. *Effect of Boron on β-Grain Morphology and β-Grain Reconstruction*

Figure 4 shows EBSD orientation maps of cross sections of laser welds of all three different Ti-64 alloys covering the BM, HAZ and FZ. Figure 4 shows the measured inverse pole figure map of (a) α phase in L-0.06 and (b, c) numerically reconstructed β phase in L-0B and L-0.06B welds. The left corner of Figure 4(a) shows the α phase morphology in the BM where α-plates form relatively large colonies. The FZ and HAZ, which have undergone a welding cycle involving rapid cooling, were found to exhibit a very fine acicular α microstructure. The transformation from β phase to α phase follows Burgers orientation relationship,[15] through which it is possible to reconstruct the prior-β grain structure. This reconstruction is shown in Figures 4(b) and (c) for the laser welds with 0.06 wt pct and 0 wt pct boron, respectively.

Table II. Dimensions of the Welds

	Weld Geometry				
	FZ Top (mm)	FZ Bottom (mm)	HAZ (mm)	Face Undercut (μm)	Root Undercut (μm)
L-0B	5.9 ± 0.3	4.9 ± 0.2	9.2 ± 0.1	170 to 250	50 to 80
L-0.06B	4.9 ± 0.1	4.4 ± 0.2	9.5 ± 0.2	20 to 60	400 to 550
L-0.11B	4.4 ± 0.3	4.0 ± 0.2	9.1 ± 0.2	80 to 200	200 to 250

Table III. Micro and Macro Hardness Results in Different Weld Zones

	Micro Hardness (HV0.5)		Macro Hardness (HV5)		
	FZ	HAZ	FZ	HAZ	BM
L-0B	339 ± 5	349 ± 8	334 ± 7	342 ± 11	309 ± 18
L-0.06B	349 ± 3	354 ± 5	337 ± 5	340 ± 5	318 ± 9
L-0.11B	351 ± 12	357 ± 10	355 ± 6	349 ± 5	328 ± 12

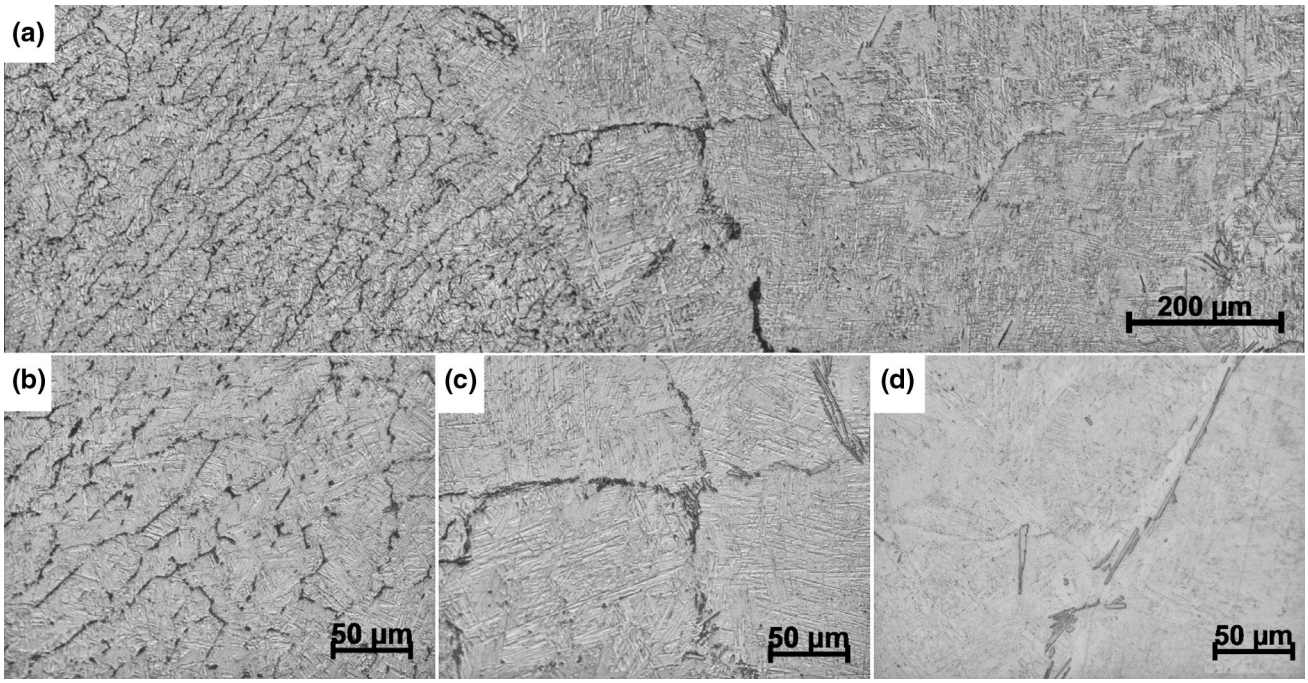

Fig. 3—Microstructure of L-0.11B: (*a*) FZ and HAZ, (*b*) FZ, (*c*) HAZ close to the fusion line, and (*d*) HAZ.

EBSD reconstruction of the β phase offers a significantly better visual impression of prior-β grains in comparison to optical microscopy, in which it was difficult to distinguish the prior-β grain boundaries in the FZ and HAZ. Table V shows the width of prior-β grains in all the welds. OM investigation showed that in the L-0B weld the prior-β grains were of the order of millimeters in size. This was also confirmed by EBSD reconstruction. Smaller β grains were also nucleated within the FZ. Boron addition refined the prior-β grain size significantly in BM, HAZ, and FZ. As shown in Figure 4(b), the size of the prior-β grains did not grow in the HAZ in comparison to the BM. TiB particles located in the prior-β grain boundaries seemed to restrict grain growth in the HAZ during welding. Smaller prior-β grain size in the HAZ also offers more nucleation sites for grains to grow in the FZ which contributed to the finer prior-β grain structure in the FZ.

The prior-β grains in the FZs of boron alloyed welds were observed to be narrow and elongated. The width of the prior-β grains in the FZs in L-0.06B was approximately 80 to 150 μm while it was 50 to 120 μm in L-0.11B. The width of the prior-β grains was larger than the spacing between the TiB stripes shown in Figure 3 and Table IV. As visible in Figure 4(b), some β grains nucleated and grew epitaxially from prior-β grains in the HAZ but there was a large number of β grains also nucleating within the FZ.

Table IV. The Volume Fraction of TiB, the TiB Stripe Spacing, and TiB Particle Size in Boron-Alloyed Welds

	TiB Volume Fraction		TiB stripe Spacing (μm)	TiB Particle Size (μm)	
L-0.06B	0.26 ± 0.07	BM 0.3 ± 0.2	21.1 ± 4	BM	length 50
L-0.11B	0.36 ± 0.12	BM 0.6 ± 0.3	20.7 ± 5		thickness 0.8 to 2
				FZ	length 10 max
					thickness 0.25

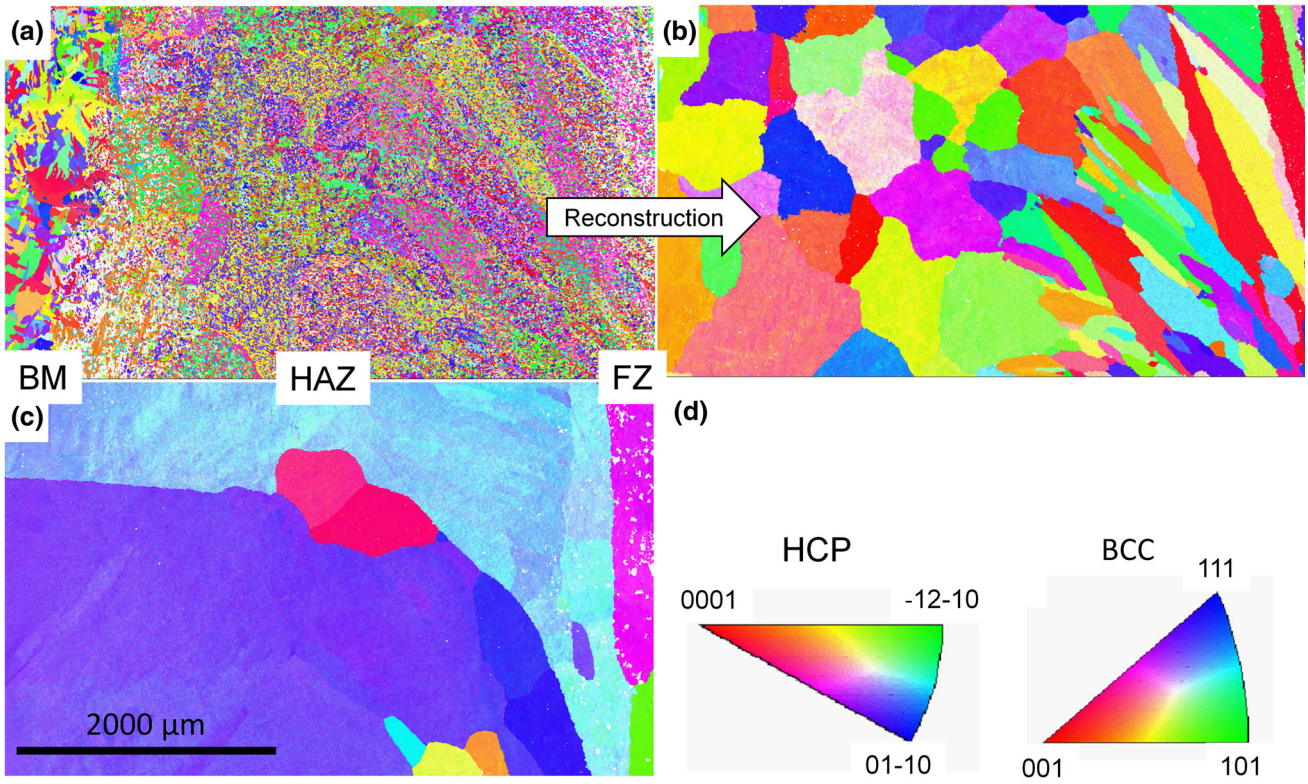

Fig. 4—EBSD maps of (*a*) the α phase in laser welded L-0.06B and reconstructed β phase in laser welded (*b*) L-0.06B, (*c*) L-0B, and (*d*) the inverse pole figure color code for the HCP α phase and the BCC β phase.

Table V. *β*-Grain Size in FZ and HAZ of the Welds

	β-Grain Size/Width (μm)	
Sample	Fusion Zone	HAZ
L-0B	> 2000	> 2000
L-0.06B	80 to 150 (250 max)	500 to 800
L-0.11B	50 to 120	400 to 700

D. α *Plate Morphology*

The microstructure in the FZs and HAZs of the welds consisted of a very fine acicular α phase separated by thin layers of β phase forming fine colony-α or Widmanstätten-type of microstructure as shown in Figure 5. TiB particles appear black in L-0.06B and L-0.11B. Boron addition was found to influence the morphology of the α-laths in the FZs of the welds. The length of α-laths decreased as boron content increased. In addition, the amount of colony type of α microstructure seemed to increase with increasing boron content. The length of α-laths in the different welds is summarized in Table VI. The α-lath thickness was found to be 0.4 to 0.5 μm in all the welds and no significant effect of boron content was observed. In boron alloyed welds, the α-lath length decreased from HAZ to FZ which is not observed in case of the standard Ti-64. The TiB particles, which act as nucleation sites for α-laths, were more evenly distributed in the FZ than in the HAZ. This contributes to the smaller α-lath length in the FZs of boron-alloyed welds.

E. *Porosity*

Porosity in the laser welds was evaluated by X-ray tomography and the 3D reconstructions of a 12-mm section of each laser weld are shown in Figure 6. The porosity is shown in red color and the surfaces of the weld specimen in gray. The pore size distributions obtained from the laser weld X-ray tomography scans are shown in Table VII. The smallest detectable pores in the X-ray tomography measurements were of

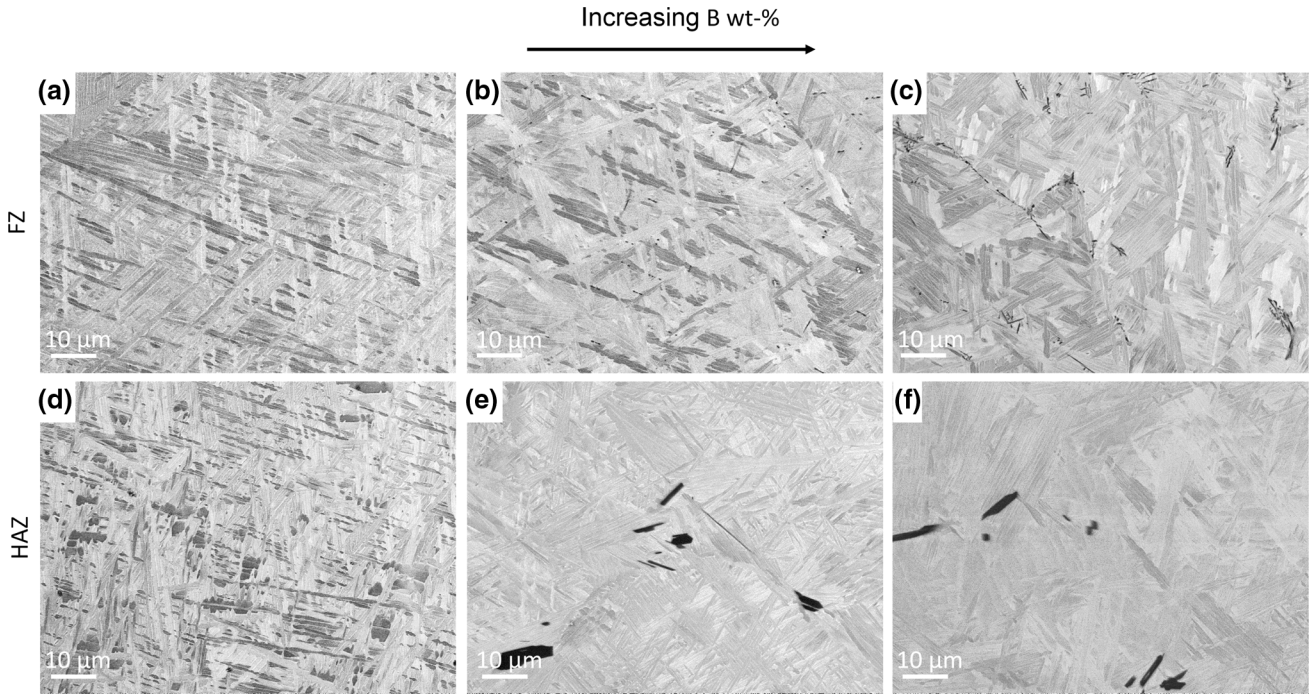

Fig. 5—SEM micrograph of the FZ in (*a*) L-0B, (*b*) L-0.06B, (*c*) L-0.11B of the HAZ in (*d*) L-0B, (*e*) L-0.06B, and (*f*) L-0.11B.

Table VI. Length of α-Laths in FZ and HAZ of the Welds

Sample	FZ (μm)	HAZ (μm)
L-0B	27 ± 8	22 ± 7
L-0.06B	18 ± 4	18 ± 4
L-0.11B	11 ± 3	17 ± 4

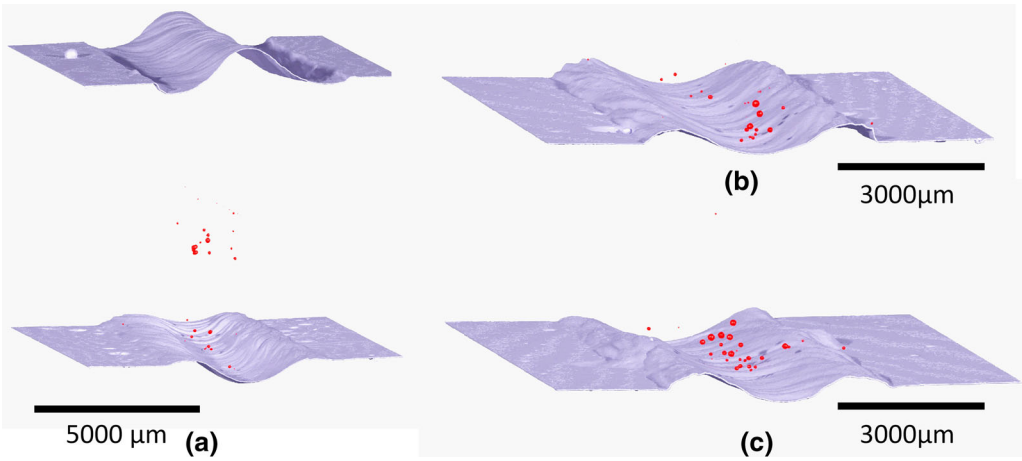

Fig. 6—3D reconstructions of 12-mm sections of (*a*) L-0B and magnified view of the root side of (*b*) L-0.06 and (*c*) L-0.11B showing the porosity in the laser welds.

approximately 20 μm size. The pores below 20 μm shown in Table VII may be noise or artifacts and were excluded from the analysis. The boron addition did not influence the size or amount of porosity. However, the location of porosity was found to be affected by boron addition. As shown in Figure 6, the porosity in the weld without boron (L-0B weld) was located mainly in the middle of the weld with some porosity evident in the root side as well. On the other hand, in the welds with boron, *i.e.*, in L-0.06B and L-0.11B, the porosity was confined to a small region along the root side of the weld. Longitudinally along the welds, the porosity was continuous and evenly distributed in all the welds.

Table VII. Pore Size Distribution in Laser Welds

	Pore size (μm)					
	< 20	20 to 50	50 to 100	100 to 150	150 to 200	> 200
L-0B	5	14	31	4	1	1
L-0.06B	8	20	35	8	1	0
L-0.11B	1	18	37	7	1	1

IV. DISCUSSION

Addition of boron in the cast base material altered the microstructure of the welds significantly. The most distinct changes that were noted included the presence of TiB particles and the refined prior-β grain size in the HAZs and FZs of the boron alloyed welds. Also, changes in α phase morphology were observed as α laths got shorter and the amount of colony type microstructure increased. This microstructural refinement with boron addition agrees well with findings of others in cast Ti-64[7–9,16] and in additive manufacturing.[9,11]

It has been well established that trace boron addition refines the prior-β grain structure in cast titanium alloys. The hypothesis by Tamiriskandala *et al.*[8] suggests that β-grain refinement is based on the growth restriction provided by boron because a boron-rich layer is formed around the solidifying β-grain. This boron enrichment causes a corresponding variation in the liquidus temperature, thereby leading to higher constitutional supercooling which provides an additional driving force for the nucleation of more fine β-grains ahead of the solid/liquid interface. The presence of equiaxed grains in boron-alloyed titanium alloy castings implies that constitutional supercooling is more important during solidification than thermal undercooling.

When a steep temperature gradient is present, as in welding or additive manufacturing, columnar growth of grains tends to occur. This was observed in the FZs of boron-alloyed welds. Bermingham *et al.*[9] explained the formation of thin elongated columnar grains by lateral solute rejection during epitaxial nucleation and growth from the BM. The presence of boron produces constitutional supercooling which restricts the lateral columnar growth and allows neighboring columnar grains to nucleate and grow. Columnar grains are also favored by the lack of potent nuclei in the melt. TiB particles that are observed in BM and FZ are initially dissolved in the melt and only precipitate during the last phase of solidification. Consequently, they do not affect the grain refinement during solidification. The grain boundary pinning effect of TiB particles may be important in restricting the β-grain growth when the temperature exceeds the β-transus temperature. This effect is apparent in the HAZs of boron-alloyed welds where no coarsening of prior-β grains was observed.

Due to the low solubility of boron in titanium, the boron that is dissolved in the melt will be rejected from the solidifying metal interface, thereby leading to local boron enrichment in the remaining melt, to promote formation of TiB particles *via* a eutectic reaction.[7,8] The formation of TiB particles has been observed in castings with slow cooling rate[6,7] as well as in additive manufacturing with high cooling rate.[9,11] In cast material, the TiB particles are mainly located at the prior-β grain boundaries. In the FZ of welds in cast boron-modified Ti-64 alloys, the TiB needles are typically clustered in the interdendritic regions and here form stripes throughout the FZ. Boron was initially added to the cast material in the form of TiB_2 particles with a size in the order of millimeters. It appears that during the casting process, these initial TiB_2 particles are completely dissolved in the melt. In the base material of the cast material, the length of TiB particles was found to be approximately 50 μm while, in the fusion zone of welds, it was approximately 10 μm. The cooling rate appears to have a significant effect on the size of the TiB particles. Bermingham *et al.*[9] approximated the cooling rate during solidification in wire arc additive manufactured Ti-64-B to be 150 Ks^{-1} based on the secondary dendrite arm spacing (approx. 25 μm) which is related to the cooling rate. In the present work, the corresponding spacing between TiB stripes, or secondary dendrite arm spacings, was approximately 20 μm, suggesting that the cooling rate during solidification was at least 150 Ks^{-1} or even slightly higher.

Titanium alloys are typically very resistant to solidification cracking because of the absence of segregating elements. Addition of boron, however, may increase the risk of liquation cracking in the HAZ during welding. Close to the fusion line (Figure 3(c)), it appears that the TiB may have partly melted/dissolved while the β-grains appear unmelted. The phase diagram for the Ti-B system[17] shows that the Ti-B eutectic has a lower melting point than pure Ti metal. This eutectic component, which segregates to the prior-β grain boundaries during solidification, could therefore risk to form a liquid film along the β-grain boundaries in the HAZ during welding. This increases the risk of liquation cracking during welding. However, no cracks were observed in this study and moreover, because the liquation cracking phenomena were not part of this study, this aspect will be further explored in future investigations. This is especially important when considering this type of alloy modifications for use in additive manufacturing, where previous layers of material are re-heated to close to the melting temperature.

Boron addition was observed to affect the morphology of α microconstituents as shown in Figure 5 and Table VI. The length of α-laths in the FZ and HAZ decreases with addition of boron. In the FZ of L-0B, the α-laths were longer and formed a typical Widmanstätten type of microstructure, whereas boron-alloyed welds contained shorter α-laths and more α-colony type of

microstructure. The refined prior-β grain size and TiB particles offer more nucleation sites for the α-phase and limit the length of α-laths and the size of α-colonies. Tamirisakandala *et al.*[18] have also shown that boron addition to Ti-64 increases the β-transus temperature which, in turn, may have an effect on the α phase morphology.

The micro and macro hardness of the welds increased slightly with the addition of boron. The hardness is mainly determined by the effective slip length which is governed by the α-colony size.[4] The presence of hard TiB particles can also increase the hardness. Here, the observed increase in hardness between unalloyed and 0.11B boron-containing welds was approximately 10 HV while the hardness of unalloyed base material was approximately 20 HV lower than the material containing 0.11 wt pct B. The difference in hardness is smaller between the weld zones than between the base materials where boron addition has a more pronounced influence on the α-colony size.

The X-ray microtomography study of the laser welds revealed no significant effect of boron on the amount or size of porosity. Pores in laser welded titanium alloys are normally considered to be related with keyhole instabilities or contamination.[19,20] However, the spatial distribution of pores was found to be different in standard grade Ti-64 when compared with the boron alloyed welds. In L-0.06B and L-0.11B, the pores were confined at the root side of the weld, whereas in L-0B the pores were found also in the middle of the weld. Boron-alloyed welds were wider than the corresponding welds of standard grade Ti-64 alloy, even though identical welding parameters were used. The face undercut was larger in L-0B than in L-0.06B and L0.11B welds. These observations are probably related to the flow of the melt pool. Boron is known to influence the melting point and solidification range of titanium alloys[7] and may have an effect on the viscosity and surface tension characteristics of the melt which therefore could influence the flow in the melt pool. However, as no experimental data are available on the exact effect boron has as an alloying element on titanium in the above respect, further discussions would be speculative.

V. CONCLUSIONS

Based on the work presented here, the following conclusions can be made:

(1) Prior-β grain reconstruction revealed the prior-β grain structure in the welds. In FZs of the welds boron refined the grain size significantly and rendered narrow columnar grains. TiB particles in the prior-β grain boundaries in the cast BM restricted grain growth in the HAZ.
(2) The length of α laths decreased and the amount of colony type α increased with boron addition. Thickness of these α laths was unaffected.
(3) The TiB particles are affected by the welding process in the fusion zone and HAZ close to the fusion line, while further in the HAZ and BM TiB particles are unaffected. The size of the affected TiB particles decreased significantly due to rapid cooling in the welding process. The TiB particles form networks of stripes along the interdendritic regions in the fusion zone of welds.
(4) FZ width and the distribution of porosity were affected by boron addition, suggesting that boron affects melt pool flow during welding.

ACKNOWLEDGMENTS

The authors would like to acknowledge the financial support of NFFP (the Swedish National Program for Aeronautical Technology) and GKN Aerospace Engine Technologies for performing welding experiments. Moreover, thanks are due to Dr. Lionel Germain at University of Lorraine for performing the β-grain reconstruction, and to Dr. Serafina Consuelo at University of Manchester and Mr. Lars Hammar at Chalmers University of Technology, respectively, for performing and helping with analyzing the results of X-ray microtomography study. Mr. Maximilian Haack (Chalmers University of Technology) is also acknowledged for his help with microscopy.

REFERENCES

1. M.J. Donachie: *Titanium A Technical Guide*, 2nd ed., ASM International, 2000.
2. K.K. Murthy, N.B. Potluri, and S. Sundaresan: *Mater. Sci. Technol.*, 1997, vol. 13, pp. 503–10.
3. T. Vilaro, C. Colin, and J.D. Bartout: *Metall. Mater. Trans. A*, 2011, vol. 42A, pp. 3190–99.
4. G. Lütjering and J.C. William: *Titanium*, Springer, New York, 2003.
5. S. Sundaresan, G.D. Janaki Ram, and G. Madhusudhan Reddy: *Mater. Sci. Eng. A*, 1999, vol. 262, pp. 88–100.
6. R. Pederson, R. Gaddam, and M.-L. Antti: *Cent. Eur. J. Eng.*, 2012, vol. 2, pp. 347–57.
7. S. Roy, S. Suwas, S. Tamirisakandala, D.B. Miracle, and R. Srinivasan: *Acta Mater.*, 2011, vol. 59, pp. 5494–5510.
8. S. Tamirisakandala, R.B. Bhat, J.S. Tiley, and D.B. Miracle: *Scr. Mater.*, 2005, vol. 53, pp. 1421–6.
9. M.J. Bermingham, D. Kent, H. Zhan, D.H. StJohn, and M.S. Dargusch: *Acta Mater.*, 2015, vol. 91, pp. 289–303.

10. S.A. Mantri, T. Alam, D. Choudhuri, C.J. Yannetta, C.V. Mikler, P.C. Collins, and R. Banerjee: *J. Mater. Sci.*, 2017, vol. 52, pp. 12455–66.
11. Z. Mahbooba, H. West, O. Harrysson, A. Wojcieszynski R. Dehoff, P. Nandwana, and T. Horn: *Jom*, 2017, vol. 69, pp. 472–78.
12. L. Germain, N. Gey, R. Mercier, P. Blaineau, and M. Humbert: *Acta Mater.*, 2012, vol. 60, pp. 4551–62.
13. J.S. Tiley, A.R. Shiveley, A.L. Pilchak, P.A. Shade, and M.A. Groeber: *J. Microsc.*, 2014, vol. 255, pp. 71–77.
14. G.Q. Wang, Z.B. Zhao, B.B. Yu, J.R. Liu, Q.J. Wang, J.H. Zhang, R. Yang, and J.W. Li: *Acta Metall. Sin. (English Lett.)*, 2017, vol. 30, pp. 499–504.
15. W.G. Burgers: *Physica*, 1934, vol. 1, pp. 561–86.
16. J. Zhu, A. Kamiya, T. Yamada, W. Shi, and K. Naganuma: *Mater. Sci. Eng. A*, 2003, vol. 339, pp. 53–62.
17. H. Okamoto: *J. Phase Equilibria Diffus.*, 2006, vol. 27, p. 303.
18. S. Tamirisakandala, R.B. Bhat, D.B. Miracle, S. Boddapati, R. Bordia, R. Vanover, and V.K. Vasudevan: *Scr. Mater.*, 2005, vol. 53, pp. 217–22.
19. J.E. Blackburn: *Understanding Porosity Formation and Prevention when Welding Titanium Alloys with 1 μm Wavelength Laser Beams*, The University of Manchester, 2011, p. 224.
20. J. Huang: *The Characterisation and Modelling of Porosity Formation in Electron Beam Welded Titanium Alloys*, The University of Birmingham, 2011, p. 180.